Picosecond soft x-ray source from subpicosecond-laser-produced plasmas

J. Workman, A. Maksimchuk, X. Liu, U. Ellenberger,

J. S. Coe, C.-Y. Chien, and D. Umstadter

Center for Ultrafast Optical Science, University of Michigan, Ann Arbor, MI 48109-2099

Phone: (313) 764-2284, Fax: (313) 763-4876

Abstract

Short-pulse, high-intensity laser-plasma interactions are investigated experimentally with temporally and spectrally resolved soft x-ray diagnostics. We demonstrate that the pulse width of the laser-produced x rays emitted from solid targets may be varied down to the picosecond time scale by adjusting the incident laser flux. Bright, picosecond, broadband emission, characteristic of a short-scale-length, high-density plasma, is produced only when a high laser contrast (10^{10}) is used. The results are found to be in qualitative agreement with both the predictions of a simple model of radiation from a collisionally dominated atomic system and the results from a numerical simulation.

07.85.Fv, 32.30.Rj, 52.25.Nr, 52.40.Nk

1. INTRODUCTION

With the development of ultrashort-pulse, high-intensity lasers,[1] studies of new plasma parameter regimes have been made possible. The interaction of these laser pulses with solid targets are unique because, during the ultrashort laser pulse, relatively little expansion occurs, and the density scale length remains much less than the laser wavelength.[2,3] This makes possible the direct deposition of a significant amount of the laser energy at near-solid density. Steep plasma temperature and density gradients cause rapid cooling, resulting in highly non-equilibrium conditions with the concurrent emission of extremely bright ultrashort x-ray pulses. These x-ray sources may be used for the study of radiation hydrodynamics or opacity in a parameter regime that is otherwise inaccessible, or for the study of time-resolved diffraction, spectroscopy, or microscopy of transient physical, chemical or biological phenomena.[4]

Methods for increasing the radiant power of x-ray sources from ultrashort-laser-produced plasmas are a topic of considerable current interest. Physical parameters that control x-ray pulse duration have been discussed in theoretical work, including the effects of plasma expansion and thermal conductivity.[5–7] Experimentally, a filtered x-ray streak camera—which provides high temporal, but only poor spectral resolution—was used to observe the decrease in x-ray pulse width with increasing laser-intensity contrast, indicating that only with high-laser contrast can the laser energy be deposited at high plasma density.[8] Techniques employed to increase laser light absorption, and hence x-ray emission, have included the use of structured targets[9] and the use of a pre-ionizing laser pulse to increase the plasma-density scale length.[10]

In this paper, we demonstrate experimentally, and explain qualitatively, a method for increasing x-ray power in a collisionally dominated plasma by decreasing the pulse duration while maintaining high x-ray emission. X-ray pulse durations can be controlled through the collision rates by controlling the incident laser intensity, and thus the peak electron temperature. Specifically, we show that a lower peak electron temperature leads to a shorter pulse of x rays, which are shown experimentally to be as short as a few picoseconds in duration. Unlike temporal studies of keV emission,[11] which require the highest laser intensities, soft x-ray emission has the advantage that it can be studied with both high temporal and spectral resolution over a large range of laser intensities ($1 \times 10^{15} \leq I \leq 5 \times 10^{17}$ W/cm^2) and, thus, over a large range of peak electron temperatures. The lower required laser intensities suggest the use of high repetition rate laser systems and, therefore, higher average power x-ray sources. We qualitatively explain our experimental results with a simple model of radiation from a collisionally dominated atomic system. Numerical results confirm the collisional dependence of the x-ray pulse duration.

The experimental arrangement used for measuring the x rays is in Sec. 2. Results of the experimental measurements are detailed in Sec. 3. In Sec. 4, we present a qualitative discussion of the factors controlling the pulse width of the x-ray emission in a collisionally dominated atomic system. In Sec. 5, we discuss the results of our detailed numerical model. Finally in Sec. 6, we present a summary.

2. EXPERIMENTAL ARRANGEMENT

In performing the experiment, we used a 400-fs terawatt Nd:glass laser system based on chirped-pulse amplification. The intensity contrast ratio of the fundamental 1.06-μm laser light, measured to be 5×10^5, was increased to approximately 10^{10} by frequency doubling. An off-axis parabolic mirror was used to focus the 2ω-laser radiation onto a solid target at normal incidence. A minimum spot size of 15 μm with an energy of about 300 mJ was achieved, corresponding to a maximum intensity in the second harmonic light of 5×10^{17} W/cm^2. Targets included 4-μm thick aluminum and gold deposited onto silicon wafers. In order to decrease the incident flux on the target, the laser spot size was defocused while keeping the total laser energy constant.

The soft x-ray emission was spectrally dispersed using an imaging flat-field grazing-incidence variable-spaced grating spectrometer located at an angle of 45 degrees to the target normal. With a spectrometer entrance slit width of 200 μm we obtained a spectral resolution, $\lambda/\Delta\lambda$, of about 300 at 50 Å. Time-resolved spectra were obtained in a single shot, using an x-ray streak camera with a potassium bromide photo-cathode supported by a Lexan film, coupled to the spectrometer. The temporal resolution was measured to be 5 ps. A 20-μm x-ray pinhole camera, filtered with 25 μm of Be and 6000 Å of Al, was used to monitor the laser spot size and emission region. Two PIN diodes filtered with 50 μm and 100 μm of Be were used to monitor relative keV x-ray emission levels and to monitor the reproducibility of each interaction. A calibrated calorimeter was used to monitor the laser energy of each shot. To obtain quantitative conversion efficiencies of the laser radiation into x rays, in the range 1.5–5 keV, DEF film was used with steps of Be filters of different thicknesses and processed using known characteristic absorption curves.[12]

3. EXPERIMENTAL RESULTS

A. Effects of Laser Contrast on X-Ray Emission

Figures 1(a) and (b) show the temporally and spectrally dispersed emission from a laser-irradiated aluminum target ($Z = 13$) for two different laser contrasts, with the same laser intensity. The x-ray amplitude is shown with a gray scale in units of CCD counts. The amplitude is plotted for both wavelength (vertical axis in units of angstroms) and time (horizontal axis in units of picoseconds). Figure 1(b) is the emission using 1.06-μm light to irradiate the target. One sees that the emission is dominated by lines and that the pulse duration is long, $\tau \sim 50$ ps (FWHM). This is characteristic of a long pulse interaction that generates a low density plasma. Figure 1(a) shows the emission using frequency doubled (0.53-μm) irradiation, corresponding to high-contrast illumination of the target. Figures 1(c) and (d) are line-outs in wavelength at the time of peak emission in the two contrast cases. Note that in the high-contrast case the emission is continuous over the entire wavelength range, characteristic of high-density spectral broadening, and that the pulse duration ($\tau \sim 15$ ps (FWHM)) is shorter than in the low-contrast case. The spectral resolution is clearly sufficient to see the effects of the high-density broadening on the line emission. In both figures, the sharp cutoff near the carbon K-edge (44 Å) is due to absorption by the Lexan film that supports the potassium bromide photo-cathode. Subsequent results are presented using the high-contrast laser pulse to obtain the shortest duration, most broadband x-ray emission.

B. X-Ray Pulse Duration and Laser Intensity

The dependence of x-ray pulse duration on laser intensity is demonstrated in Fig. 2, which shows single-shot aluminum x-ray emission for three different laser intensities, ranging from 2.0×10^{17} down to 2.0×10^{15} W/cm^2 in the wavelength range of 45 to 70 Å. The obvious trend is the decrease in x-ray pulse duration with decreasing laser intensity. High-density effects at early times are quite obvious in all cases, as the initial Stark-broadened emission is virtually continuous over the entire wavelength region shown.

Figure 3 shows a comparison of amplitude-normalized temporal profiles from the above plots of the Al XI $2p$-$3d$ emission line ($\lambda = 52.4$ Å) obtained for 2ω-irradiation for a range of laser intensities. Again, one clearly sees the pronounced decrease of the x-ray pulse duration as the laser intensity is decreased. The rise time is short in all cases as expected from the rapid heating. (The starting positions of the plots relative to the laser pulse and each other are unknown.) The fall time is observed to be shorter and the slope of the decay much steeper in the lowest-laser-intensity case. Similar results were obtained for the Al XI $2s$-$3p$ transition as well as for other Al XI transitions in this wavelength region. In the keV region, an increase in x-ray yield (normalized to the emission volume) was observed with increasing laser intensity, implying a corresponding increase in electron temperature.

Results of the gold emission in this wavelength region are shown in Fig. 4. The gold x-ray pulse durations are found to be even shorter than the aluminum emission at similar laser intensities. This is presumably due to the higher electron densities, that one would expect in a high Z material such as gold, which lead to higher collision rates. The emission from the gold is extremely continuous even at late times, due to the high density of emission lines in this spectral region.

Figure 5 shows the comparison of measured x-ray pulse duration as a function of laser flux for the two materials aluminum and gold. The averaged experimental aluminum pulse widths at $\lambda = 52.4$ Å are shown as crosses. The gold data, also at $\lambda = 52.4$ Å is represented by the open diamonds. The data was averaged over three to five laser shots with the standard deviation of the pulse duration shown by the vertical error bars. Horizontal error bars indicate spot size uncertainty, as measured by our pinhole camera and, at low laser energy (about 0.5 mJ), by optical techniques. For the same laser intensity, the gold x-ray pulse duration was found to be as little as half the aluminum pulse duration and was streak-camera-limited at the lowest intensity. This is presumably due to the higher electron densities that one would expect in a high-Z material such as gold, which lead to faster cooling rates.

Conversion efficiency measurements were made for both the gold and aluminum targets for the x-ray photons with $h\nu \geq 1$ keV. For a laser intensity of 1×10^{17} W/cm^2 the conversion efficiency reached about 0.1 percent (up to one mJ) for the gold target. Conversion efficiency for the gold target was found to be four times higher than for the aluminum target, due to the higher density of emission lines in this spectral region. Because of the shorter pulse duration and higher conversion efficiency the gold emission is almost ten times brighter than the aluminum emission.

4. THEORY

The duration of x-ray line emission from a plasma ion is determined primarily by the dynamics of its lifetime and electron energy-level populations. At high plasma density, these factors depend on the rate of collisions between free electrons and ions. Because of the experimentally observed predominance of line emission, we will not discuss the minor contribution of radiative two-body recombination in this wavelength region.

The rise time of the x-ray pulse is roughly determined by the plasma heating time. In the absence of radiative heating, a given region of the plasma is heated either by direct deposition of laser energy or by diffusion of heat from neighboring regions. The decay of the x-ray emission will be controlled by cooling processes, which include both expansion into the vacuum and heat conduction into the colder regions of the solid. For a particular ion, bound-bound emission from any local region of the plasma, at any given time, is determined by the population densities of the various allowed energy levels. More precisely, the emission will be determined by the source function, defined as the emissivity divided by the opacity, ϵ/κ.[13] The temporal behavior of the source function depends almost linearly on the time history of n_u/n_l, where n_u and n_l are the upper and lower state densities of the transition considered. (As n_u/n_l approaches one, the dependence is only slightly non-linear.) The time history of the emission is then determined by the time history of the upper- and lower-state density ratio. In what follows, we will consider a simple analytic model that describes the time history of two bound states in a highly collisional plasma.

We can consider a system with two bound states, consisting of n_u and n_l, and a free electron state. For the conditions of our experiment, lithium-like ions at high density (which gives rise to continuum lowering), this system is not unreasonable. Because of the high densities produced in these plasmas, we will neglect contributions of rates containing radiation fields, as they are generally much less than the collision rates, at the temperatures considered here ($T_e < 1$ keV). We can consider two bound-bound collision rates: one, responsible for exciting an electron from n_l to n_u, and the other, for de-exciting an electron in n_u down to n_l. The de-excitation rate per ion is proportional to $n_e/\sqrt{T_e}$, and the excitation rate per ion is proportional to $n_e \exp(-h\nu_{ul}/kT_e)/\sqrt{T_e}$.[14] Therefore, the difference between these two rates is controlled by the factor $\exp(-h\nu_{ul}/kT_e)$. Collisional ionization and recombination account for transitions from bound to free and free to bound states respectively. The net recombination into any bound level scales as $\exp(\chi/kT_e)$, where χ is the ionization potential.[15] Therefore the net rate of change of the bound populations, due to recombination, again scales as $\exp(-h\nu_{ul}/kT_e)$. We see that the higher the electron temperature, the smaller the difference between the two rates and, therefore, the smaller the change in the ratio n_u/n_l for a given change in the electron temperature. A high peak electron temperature would mean a slow decrease in emission, which changes linearly with the population ratio, and, therefore, a long pulse duration, for a given cooling rate. As the electron temperature decreases, the difference between the rates begins to change more rapidly. The pulse-duration dependence on temperature predicted above explains the experimental results of Fig. 3, in which the x-ray pulses under high-laser-intensity conditions are longer in duration than under conditions of low laser intensity.

A. Maximizing Radiant Power

Of course, if the temperature is kept too low for a particular band of radiation, the x-ray intensity will be greatly reduced because the proportion of ions responsible for emission, in a particular spectral region, will be smaller.[16] This means that to obtain short, high fluence x-ray pulses, of a given photon energy, there exists an optimal electron temperature, and thus an optimal laser intensity.

In order to maximize the total x-ray emission, the total number of x-ray emitters should be maximized. This can be done by maximizing both the plasma density and the radial dimensions of the region over which the optimal temperature conditions exist. The former means that the shortest laser pulse should be used, in order to increase the direct deposition of laser energy at solid density. The latter implies that the laser spot size should be maximized, while keeping the peak laser intensity equal to its optimal value for the laser energy available. While the experimental results presented were obtained on a high energy low-repetition rate laser system, the shortest pulses were obtained for the lowest laser intensities. Because of the low laser intensities required the average power of these x-ray sources could easily be increased by using high repetition rate laser systems (10 Hz or greater).

B. Global Effects

The factors involved in controlling the x-ray pulse duration, described above, involve plasma conditions locally, where the x rays originated. However, due to finite plasma size, a detector external to the plasma will integrate the contributions from each local region along the radiation propagation path. Thus, absorption, re-emission, escape, stimulated emission and Doppler shifts must also be considered, which, by coupling the radiation from separate regions, makes the problem a global one. The temporal and spectral characteristics of the observed x-ray emission are determined by the complex interplay between these global effects and local plasma conditions. Since these effects are both time- and space-dependent, the complexity of the problem is well suited to detailed numerical analysis.

5. NUMERICAL ANALYSIS

A. Numerical Model

The collisional dependence discussed in Sec. 4 is demonstrated by the results of a numerical analysis of the interaction. Our one-dimensional hydrodynamics code solves the conservation equations of energy, momentum, and mass for a two-fluid plasma. The fluid equations are coupled self-consistently to the Helmholtz equation of the laser field for energy and momentum deposition in the plasma. An average-atom non-LTE model[17] is used to determine the ionization balance as a function of temperature and density. Thermal conductivity is determined by the Spitzer formula with tabulated values for low temperatures.[18] A heat flux limiter is set to one-tenth the free-streaming velocity.[19] The output of the hydrodynamics code, plasma density, and temperature of each cell, is then used as input to a detailed-configuration, time-dependent, atomic-physics package, FLY,[20] to calculate the population densities and ultimately the spectral emission. Included in the atomic physics package are the effects of Stark broadening and local opacity. A Planckian radiation field is used to determine photo-excitation and stimulated emission rates. The integrated emission along z is determined by transporting the emission from each cell through the plasma while incorporating the effects of opacity and translational Doppler shifts. Global effects of opacity are determined by the simple equation, $I_{o(n+1)} = I_{o(n)}(1 - exp(\kappa L)) + I_{n+1}$, where $I_{o(n+1)}$ is the total emission intensity after traversing cell $n+1$, $I_{o(n)}$ is the total emission intensity after traversing the previous cell and I_{n+1} is the emission originating in cell $n+1$. κ is the frequency-dependent opacity of cell $n+1$ and L is the length of cell $n+1$.

Results of the numerical analysis predict a pulse duration of 2.2 ps for the AlXI $2p$-$3d$ doublet at $\lambda = 52.4$ Å at a laser intensity of 5×10^{17} W/cm^2, and a pulse duration of 1.9 ps at a laser intensity of 5×10^{16} W/cm^2. The peak electron temperature was found to be about 1 keV for the highest intensity case and about 400 eV for the 5×10^{16} W/cm^2 case. As expected, the predicted pulse duration becomes shorter as the laser intensity is decreased in the simulation.

The effects of Doppler shifts on the line transport were found to be extremely small, due to Stark broadening at high density. Opacity played a very large role in the line transport, reducing the pulse duration from 20 ps to 2 ps at a laser intensity of 10^{17} W/cm^2. Values of line opacity remained above 10^4 cm^{-1} for up to 20 picoseconds in the middle and outer regions of the plasma due to the fast expansion and thus long ionization lifetimes. Emission from the higher density inner regions did not escape leaving the outer lower density regions as the only source of emission, reducing the intensity considerably. The probability of re-emission of the absorbed radiation at the same wavelength was estimated to be less than 5 percent in almost all regions of the plasma due to the dominance of the collision rates over the 1 ps spontaneous rate for this transition (AlXI $2p - 3d$).[21] Having obtained very similar results for the AlXI $2s - 3p$ transition (at 48.3Å), we will instead concentrate on the AlXI $2p - 3d$ transition.

B. Analysis of Numerical Results

Because the integrated output of the numerical simulation is very sensitive to the radiation transport model used, it will be more useful to look at the summed emission along the z axis without the effects of opacity. Figure 6 shows the numerical results of the integrated, normalized x-ray emission as a function of time for three different laser intensities, without the effects of radiation transport. The emission is averaged over a spectral range of 52.2 to 52.5 Å to simulate the resolution of the spectrometer used in the experiment. Figure 6 shows that the tail of the pulse has a more gradual slope at higher laser intensity and becomes steeper as the laser intensity is decreased. The longer x-ray pulses correspond to higher average electron temperatures as expected. As we have seen in Fig. 3, there is a similar trend in the experimentally measured pulse tails. The qualitative similarities between experiment and simulation both agree with the simple atomic model presented.

Several obvious reasons for quantitative discrepancy between simulation and experiment can be suggested. Our simple numerical model for opacity may be quite inadequate to describe the radiation transport in this highly non equilibrium, high-density plasma. Large magnetic fields[22] might also influence the dynamics of the plasma, and therefore the emission. The effects of magnetic fields would be extremely difficult to include in a one-dimensional simulation. Current laser absorption, equation-of-state and thermal conductivity models may also be inaccurate for these types of plasmas. Contributions from detailed Be-like satellite emission, which might have some contribution in the red wings of the Li-like transition that we have considered, are not included in our atomic physics package. Regardless of the current lack of a comprehensive model for emission from these unique plasmas, our results confirm that the pulse duration, as a function of laser intensity, is controlled by the temperature dependence in the collision rates. Therefore, bright picosecond x-ray emission can be obtained by controlling the plasma temperature through an appropriate choice of high-contrast laser intensity.

6. SUMMARY

To summarize, we have shown that the pulse width of soft x rays emitted from these high-density plasmas is controlled by the temperature dependence of the collision rates. Consequently, the pulse duration may be reduced—while increasing the areal emission region—by adjusting the laser focal spot size, and thereby the incident laser intensity. These experimental results are found to agree with a simple atomic model, and to be in qualitative agreement with the predictions of our hydrodynamics code coupled to an atomic physics model. Further, we have shown that only with a high-contrast laser pulse can one obtain short pulses of x rays. The conversion efficiency of the high-contrast subpicosecond laser pulses into ultrashort soft x-ray pulses can be as high as a few tenths of a percent. The emission from gold targets in the x-ray region of 50 Å was observed to be an-order-of-magnitude brighter than the emission from the aluminum due both to the higher conversion efficiency and the shorter pulse duration. These results illuminate the potential use of these x-ray sources as unique ultrashort probes.

7. ACKNOWLEDGMENTS

This work was partially funded by the National Science Foundation Center for Ultrafast Optical Science, contract #PHY8920108. The authors would like to thank G. Mourou, R. Lee, and J. Apruzese for useful discussions.

REFERENCES

1. G. Mourou and D. Umstadter, "Development and applications of compact high-intensity lasers," Phys. Fluids B **4**, 2315 (1992).

2. H. M. Milchberg, R. R. Freeman, S. C. Davey and R. M. More, "Resistivity of a simple metal from room temperature to 10^6 K," Phys. Rev. Lett. **61**, 2364 (1988).

3. M. M. Murnane, H. C. Kapteyn, R. W. Falcone, in *Short Wavelength Coherent Radiation: Generation and Application*, R. W. Falcone and J. Kirz, eds. (Optical Society of America, Washington, DC, 1989), **2**, 189.

4. *OSA Proceedings on Short Wavelength Coherent Radiation: Generation and Applications, 1991*, P. Bucksbaum and N. Ceglio, eds. (Optical Society of America, Washington, DC, 1991).

5. M. M. Murnane, H. C. Kapteyn, M. D. Rosen and R. W. Falcone, "Ultrafast x-ray pulses from laser-produced plasmas," Science **251**, 531 (1991).

6. H. Milchberg, I. Lyubomirsky, and C. G. Durfee, III, "Factors controlling the x-ray pulse emission from an intense femtosecond laser-heated solid," Phys. Rev. Lett. **67**, 2654 (1991).

7. S. E. Harris and J. D. Kmetec, "Mixed-species targets for femtosecond-time-scale x-ray generation," Phys. Rev. Lett. **61**, 62 (1988).

8. M. M. Murnane, H. C. Kapteyn, R. W. Falcone, "High-density plasmas produced by ultrafast laser pulses," Phys. Rev. Lett. **62**, 155 (1989).

9. M. M. Murnane, H. C. Kapteyn, S. P. Gordon, J. Bokor, E. N. Glytsis, R. W. Falcone, "Efficient coupling of high-intensity subpicosecond laser pulses into solids," Appl. Phys. Lett. **62**, 1068 (1993).

10. D. G. Stearns, O. L. Landen, E. M. Campbell, and J. H. Scofield, "Generation of

ultrashort x-ray pulses," Phys. Rev. A **37**, 1684 (1988).

11. J. C. Kieffer, M. Chaker, C. Y. Cote, Y. Beaudoin, H. Pepin, C. Y. Chien, S. Coe, G. Mourou, "Time reolved kiloelectron-volt spectroscopy of ultrashort plasmas," App. Opt. **22**, 4247 (1993).

12. B. L. Henke, P. Lee, T. J. Tanaka, R. L. Shimabukuro, B. K. Fujikawa, "Low-energy x-ray interaction coefficients: Photoabsorption, scattering and reflection," At. Data Nuc. Data Tables **27**, 1 (1982); S. L. Kwok, J. Y. Uejio, B. L. Henke, "Low-energy x-ray response of photographic films. Mathematical models," J. Opt. Soc. Am. B **3**, No. 11, 1540 (1986).

13. D. Mihalas, *Stellar Atmospheres* (W. H. Freeman and Company, San Francisco, 1978).

14. H. Van Regemorter, "Rate of collisional excitation in stellar atmospheres," Astrophys. J. **136**, 906 (1962); D. M. Cochrane and R. W. P. McWhirter, "Collisional excitation rate coefficients for lithium-like ions," Physica Scripta **28**, 25 (1983).

15. R. H. Huddlestone and S. L. Leonard, *Plasma Diagnostic Techniques* (Academic Press, New York, 1965).

16. The proportion of ions responsible for emission in a particular spectral region also will be reduced if the temperature is too high.

17. S. J. Rose, J. Quant. Spectrosc. Radiat. Transfer **36**, 389 (1986).

18. L. Spitzer, *Physics of Fully Ionized Gases* (Interscience, New York, 1962).

19. Several values for the flux limiter were used, ranging from 0.1 to 0.5, but were found to have limited effect on the overall pulse duration of the x rays.

20. R. W. Lee, B. L. Whitten, and R. E. Stout, II, "SPECTRA–a model for K-shell spectroscopy," J. Quant. Spectrosc. Radiat. Transfer **32**, 91 (1984).

21. J. P. Apruzese, "Escape time of heliumlike α resonance-line photons emitted from op-

tically thick plasmas," Phys. Rev. E **47**, 2798 (1993).

22. R. N. Sudan, "Mechanism for the generation of 10^9 G magnetic fields in the interaction of ultraintense short laser pulse with an overdense plasma target," Phys. Rev. Lett. **70**, 3075-8 (1993).

FIGURES

Fig. 1. Streaked aluminum x-ray spectra obtained in a single shot with a high-resolution grazing-incidence spectrometer: (a) and (c) using 2ω laser irradiation, corresponding to high-contrast conditions; (b) and (d) ω laser irradiation, corresponding to low-contrast conditions. Spectral line-outs (c) and (d) are taken at the peak of emission.

Fig. 2. Temporally and spectrally resolved aluminum x-ray emission obtained for three different laser intensities.

Fig. 3. Comparison of amplitude-normalized temporal profiles of the AlXI $1s^2 2p - 1s^2 3d$ transition obtained experimentally, showing the reduction of pulse duration with decreasing laser intensity.

Fig. 4. Temporally and spectrally resolved gold x-ray emission obtained experimentally.

Fig. 5. Duration of the x-ray emission, at ($\lambda = 52.4$ Å), versus laser intensity as measured experimentally: aluminum (crosses) AlXI $2p - 3d$, gold (diamonds).

Fig. 6. Comparison of amplitude-normalized spatially integrated temporal profiles of the AlXI $1s^2 2p - 1s^2 3d$ emission obtained numerically. Note: emission does not include the effects of opacity.

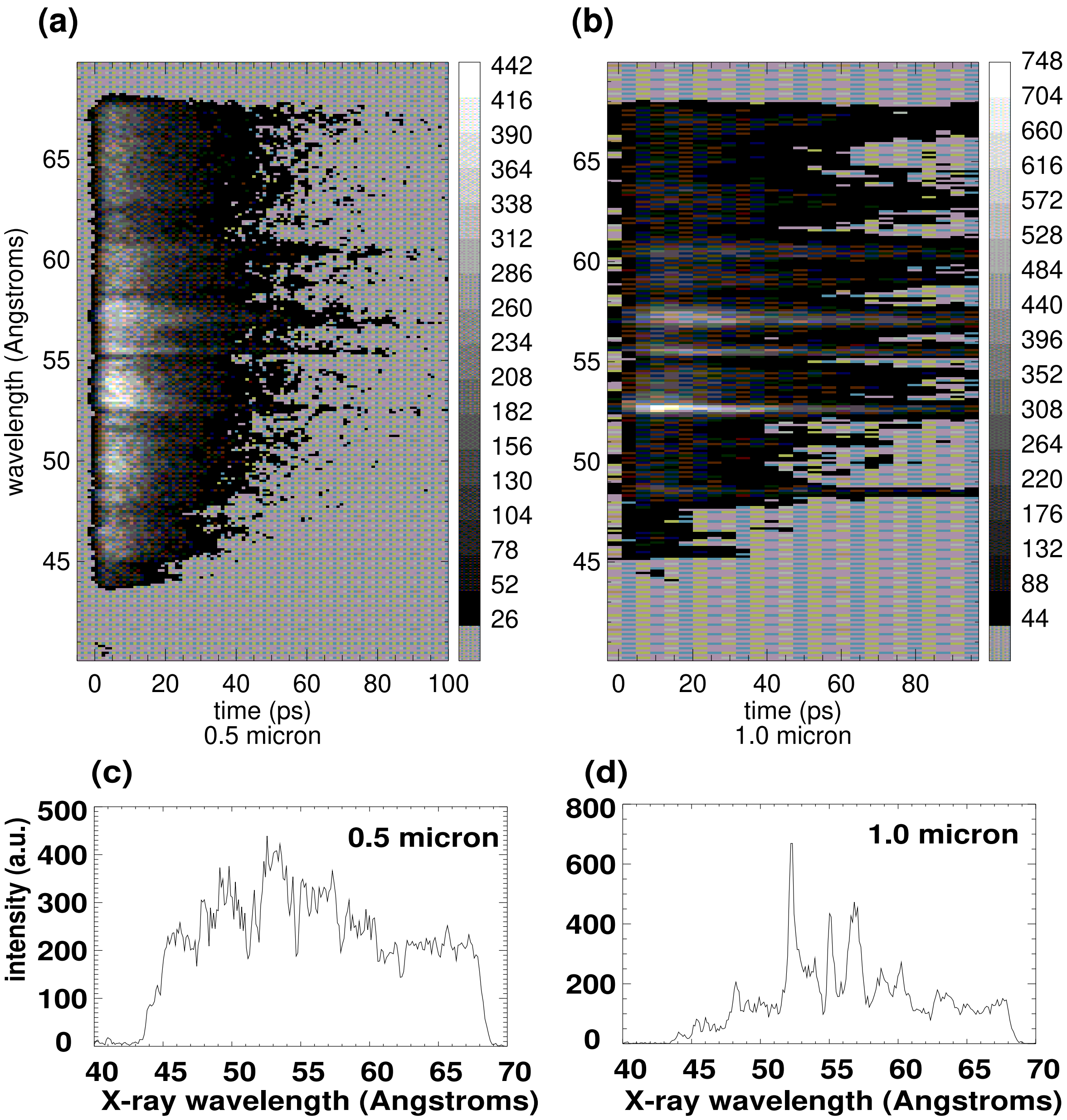

(a)
(b)
wavelength (Angstroms)
time (ps)
0.5 micron
1.0 micron
(c)
(d)
intensity (a.u.)
0.5 micron
1.0 micron
X-ray wavelength (Angstroms)
X-ray wavelength (Angstroms)

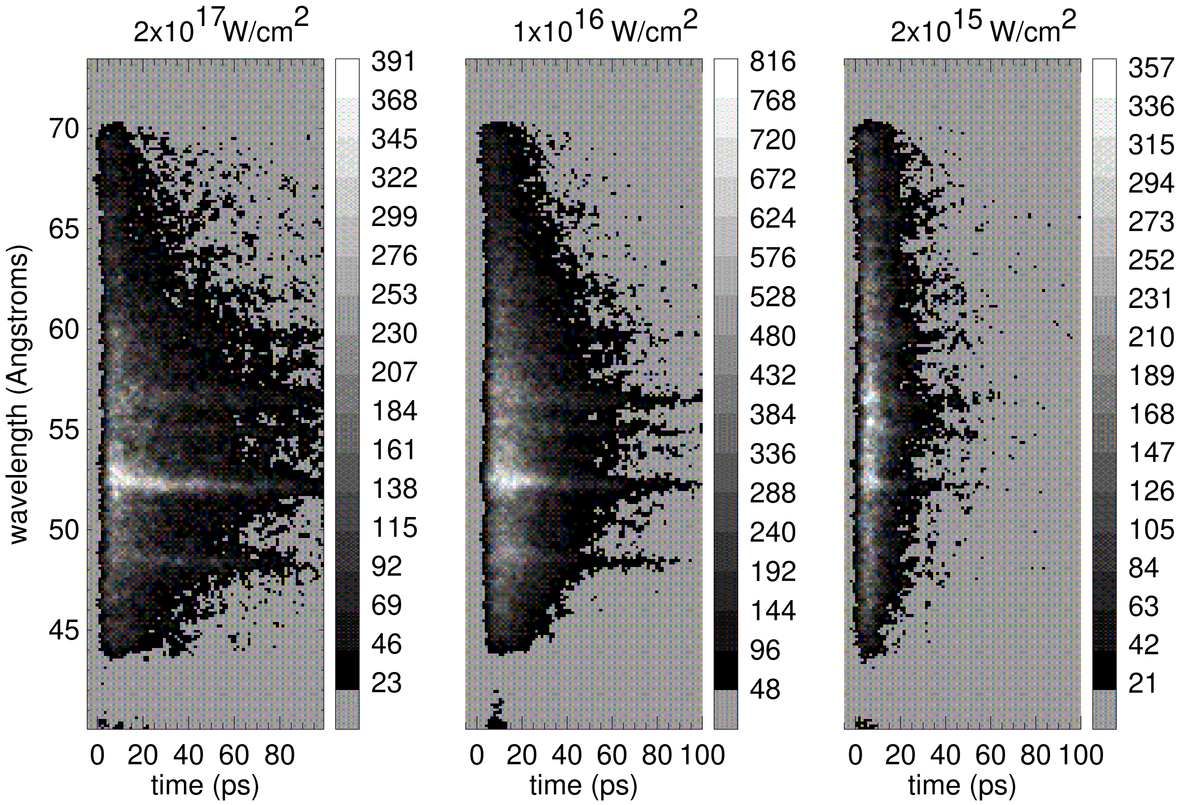
2x10^17 W/cm^2
1x10^16 W/cm^2
2x10^15 W/cm^2
wavelength (Angstroms)
time (ps)
time (ps)
time (ps)
70
65
60
55
50
45
0 20 40 60 80
0 20 40 60 80 100
0 20 40 60 80 100
391 368 345 322 299 276 253 230 207 184 161 138 115 92 69 46 23
816 768 720 672 624 576 528 480 432 384 336 288 240 192 144 96 48
357 336 315 294 273 252 231 210 189 168 147 126 105 84 63 42 21

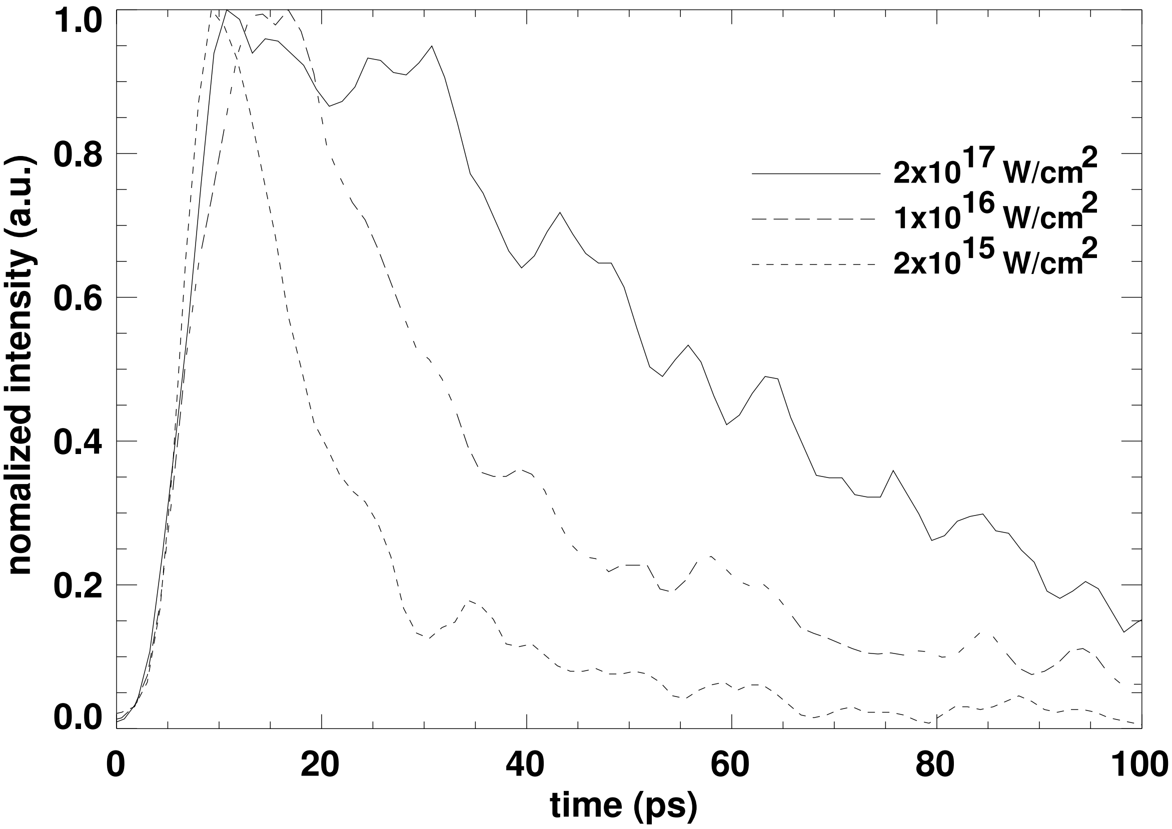
1.0
0.8
0.6
0.4
0.2
0.0
0
20
40
60
80
100
time (ps)
nomalized intensity (a.u.)
2x10^17 W/cm^2
1x10^16 W/cm^2
2x10^15 W/cm^2

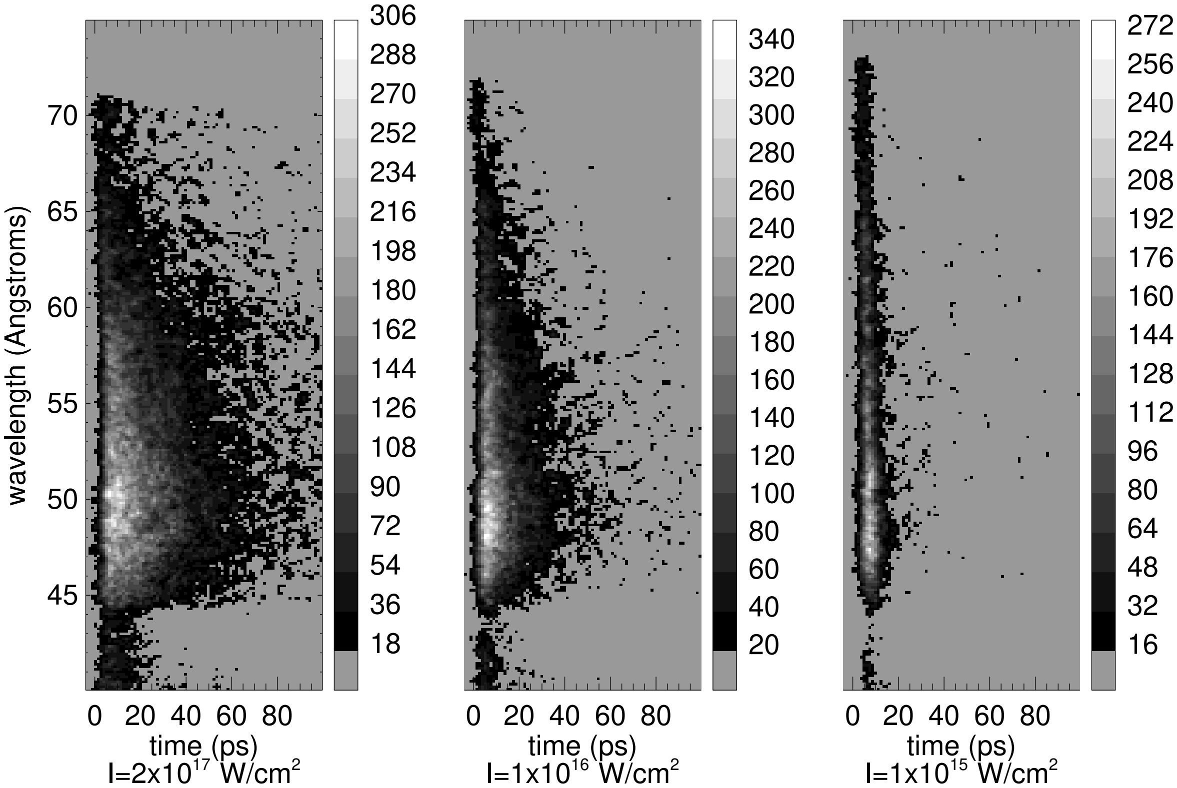
wavelength (Angstroms)
70
65
60
55
50
45
0 20 40 60 80
time (ps)
I=2x10^17 W/cm^2
306 288 270 252 234 216 198 180 162 144 126 108 90 72 54 36 18
0 20 40 60 80
time (ps)
I=1x10^16 W/cm^2
340 320 300 280 260 240 220 200 180 160 140 120 100 80 60 40 20
0 20 40 60 80
time (ps)
I=1x10^15 W/cm^2
272 256 240 224 208 192 176 160 144 128 112 96 80 64 48 32 16

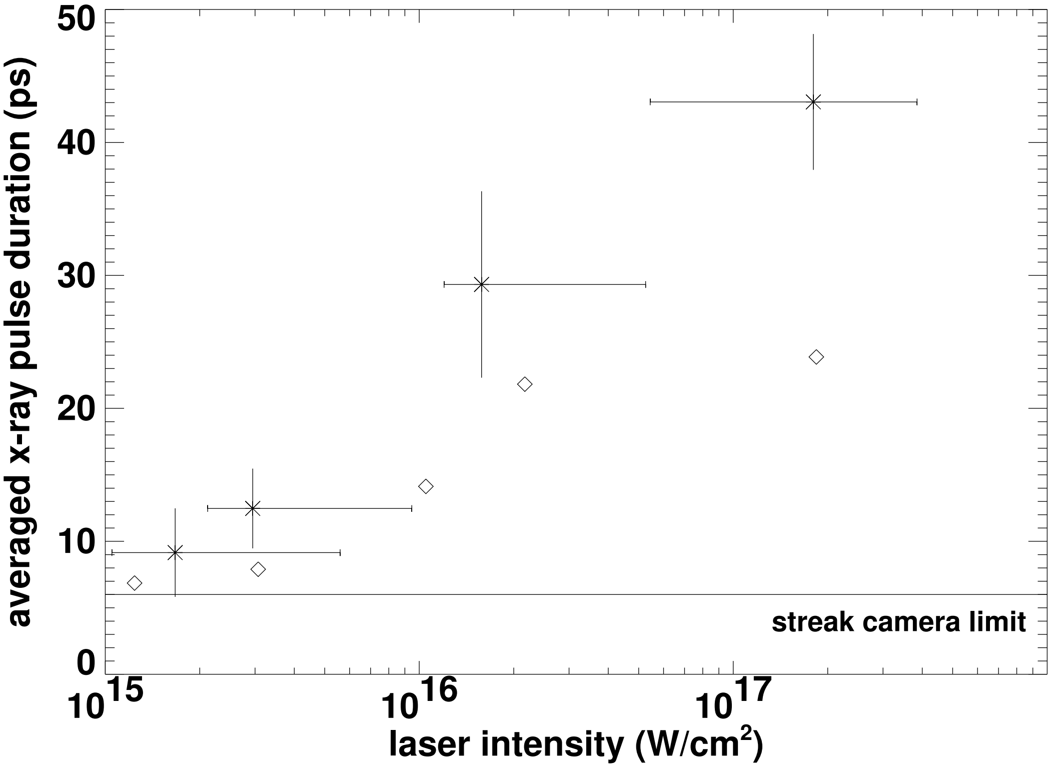
averaged x-ray pulse duration (ps)
0
10
20
30
40
50
10^{15}
10^{16}
10^{17}
laser intensity (W/cm^2)
streak camera limit

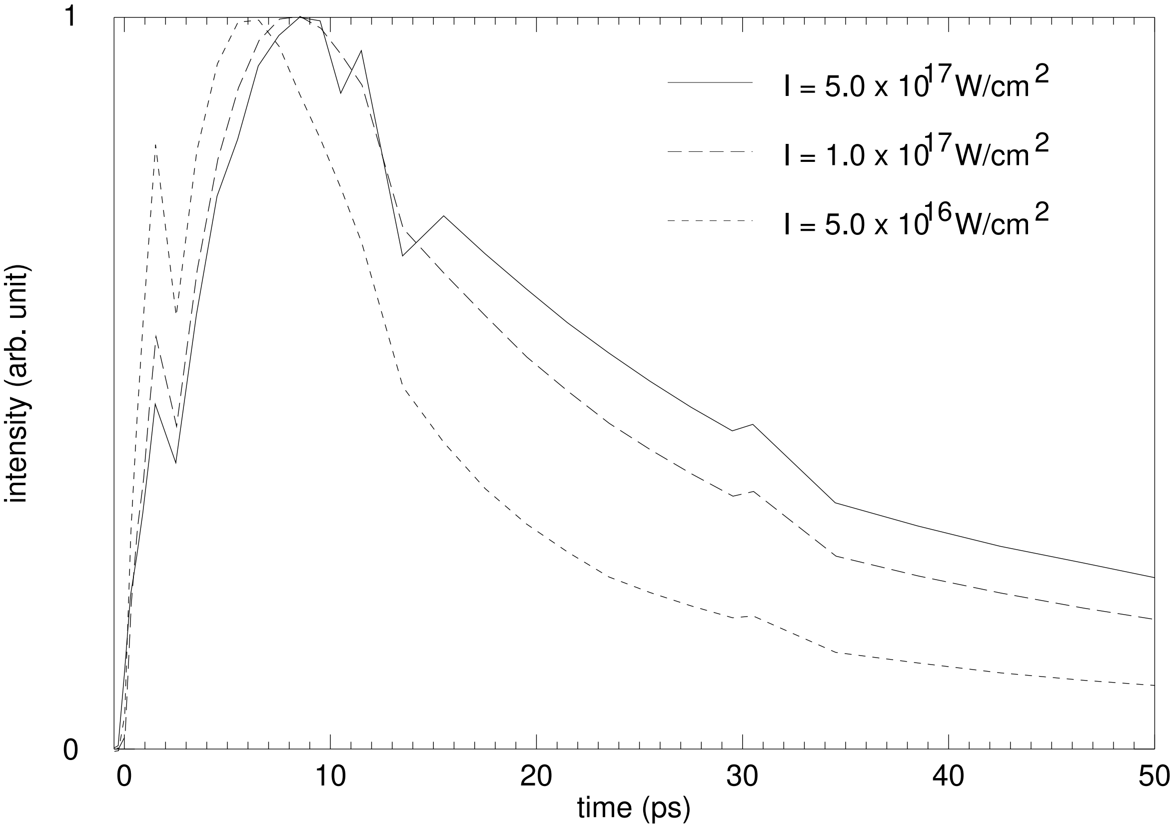
1
0
intensity (arb. unit)
0
10
20
30
40
50
time (ps)
I = 5.0 x 10^{17}W/cm^{2}
I = 1.0 x 10^{17}W/cm^{2}
I = 5.0 x 10^{16}W/cm^{2}